Journal of Marine Science and Technology

Volume 26 | Issue 6 Article 5

A SIMPLIFIED TWO-SWITCHING-BASED MODEL-FREE PREDICTIVE CURRENT CONTROLLER FOR AN INTERIOR PERMANENT MAGNET SYNCHRONOUS MOTOR DRIVE SYSTEM

Cheng-Kai Lin
Department of Electrical Engineering, National Taiwan Ocean University, Keelung, Taiwan, R.O.C,
cklin@mail.ntou.edu.tw

Jen-te Yu
Department of Electrical Engineering, Chung Yuan Christian University, Taoyuan, Taiwan, R.O.C

Jyun-Ting Wang
Department of Electrical Engineering, National Taiwan Ocean University, Keelung, Taiwan, R.O.C

Yen-Shin Lai
Department of Electrical Engineering, National Taipei University of Technology, Taipei, Taiwan, R.O.C.

Hsing-Cheng Yu
Department of Systems Engineering and Naval Architecture, National Taiwan Ocean University, Keelung, Taiwan, R.O.C

See next page for additional authors

Recommended Citation

Lin, Cheng-Kai; Yu, Jen-te; Wang, Jyun-Ting; Lai, Yen-Shin; Yu, Hsing-Cheng; and Huang, Hao-Qun (2018) "A SIMPLIFIED TWO-SWITCHING-BASED MODEL-FREE PREDICTIVE CURRENT CONTROLLER FOR AN INTERIOR PERMANENT MAGNET SYNCHRONOUS MOTOR DRIVE SYSTEM," *Journal of Marine Science and Technology*: Vol. 26: Iss. 6, Article 5.
DOI: 10.6119/JMST.201812_26(6).0005
Available at: https://jmstt.ntou.edu.tw/journal/vol26/iss6/5

A SIMPLIFIED TWO-SWITCHING-BASED MODEL-FREE PREDICTIVE CURRENT CONTROLLER FOR AN INTERIOR PERMANENT MAGNET SYNCHRONOUS MOTOR DRIVE SYSTEM

Acknowledgements

This manuscript is a result of joint research sponsored by the Ministry of Science and Technology of Taiwan, National Taiwan Ocean University, Chung Yuan Christian University, and National Taipei University of Technology under grant numbers MOST 107-2221-E-019-040, MOST 107-2221-E-033-062, and USTP-NTUT-NTOU-107-01. The authors thank these institutions for their support.

Authors

Cheng-Kai Lin, Jen-te Yu, Jyun-Ting Wang, Yen-Shin Lai, Hsing-Cheng Yu, and Hao-Qun Huang

Journal of Marine Science and Technology, Vol. 26, No. 6, pp. 803-812 (2018)
DOI: 10.6119/JMST.201812_26(6).0005

A SIMPLIFIED TWO-SWITCHING-BASED MODEL-FREE PREDICTIVE CURRENT CONTROLLER FOR AN INTERIOR PERMANENT MAGNET SYNCHRONOUS MOTOR DRIVE SYSTEM

Cheng-Kai Lin[1], Jen-te Yu[2], Jyun-Ting Wang[1],
Yen-Shin Lai[4], Hsing-Cheng Yu[3], and Hao-Qun Huang[1]

Key words: predictive current controller, interior permanent magnet synchronous motor, voltage source inverter.

ABSTRACT

This paper presents a simplified two-switching-based model-free predictive current control (STSB-MFPCC) method as well as its application to interior permanent magnet synchronous motor (IPMSM) drive systems. Unlike existing model predictive current controller (MPCC) that uses 7 basic voltage vectors, STSB-MFPCC employs 19 synthesized ones, with each of which consisting of two basic voltage vectors. The new method does not require any information about the load parameters, back electromotive force, nor the system model. Compared to model-based controllers, the proposed one has a distinctive and appealing nature in that it is much less sensitive to system parameter variations. A digital signal controller, TMS320F28377S, is used to realize and validate the new method and verifies its feasibility as well as performance saliency.

I. INTRODUCTION

Current control schemes, commonly used in interior permanent magnet synchronous motor in recent years, can be classified into three types: hysteretic current control (Bolognani et al., 2011), pulse width modulation (PWM) control (Kadota et al., 2007; Gu et al., 2016), and predictive current control (PCC) (Rodríguez et al., 2007). The first two, as limited by their natures, cannot predict future currents in the next sampling period. Due to its simplicity and ease of implementation, the PCC algorithm of 2007 (Rodríguez et al., 2007) has been studied extensively, including a large amount of publications that followed, and has become one of the most popular research topics ever since. It results from the fact that the PCC can predict the load currents of the inverter for all possible switching modes in the next period, and then finds an optimal one to use.

The PCC exhibits good characteristics in computer simulations, including low current ripple, low steady-state current error, and fast transient response. As the PCC (Rodríguez et al., 2007; Zhang et al., 2018) is based on discrete-time mathematical models, its performance will be noticeably affected by the uncertainties and/or variations of the load parameters and the estimation error of the back electromotive force, which in turn result in performance degradation in practice. Notice that nonlinear phenomena in real systems cannot be neglected.

Recently, model-free predictive current controllers (MFPCCs) (Lin et al., 2014; Chen et al., 2015; Lin et al., 2016a; Lin et al., 2016b; Lin et al., 2018; Lin et al., 2018) were proposed to improve the drawbacks of MPCCs (Rodríguez et al., 2007; Mwasilu et al., 2018), as they do not need any information about the inductance, the resistance, nor the back EMF but still have good performance. It is worth noting that the MFPCC requires the use of analog-to-digital (A/D) converter of high resolution, typically of 16 bits at least. In order to reduce the hardware cost yet retaining current tracking performance, a simplified two-switching-based model-free predictive current controller (STSB-MFPCC) is proposed in this paper.

Compared to existing predictive current control that uses 7 voltage vectors, the proposed approach uses 19 synthesized ones. The stator current will be detected twice in a sampling period

Paper submitted 06/07/18; revised 10/04/18; accepted 11/05/18. Author for correspondence: Cheng-Kai Lin (e-mail: cklin@mail.ntou.edu.tw).
[1] *Department of Electrical Engineering, National Taiwan Ocean University, Keelung, Taiwan, R.O.C.*
[2] *Department of Electrical Engineering, Chung Yuan Christian University, Taoyuan, Taiwan, R.O.C.*
[3] *Department of Systems Engineering and Naval Architecture, National Taiwan Ocean University, Keelung, Taiwan, R.O.C.*
[4] *Department of Electrical Engineering, National Taipei University of Technology, Taipei, Taiwan, R.O.C.*

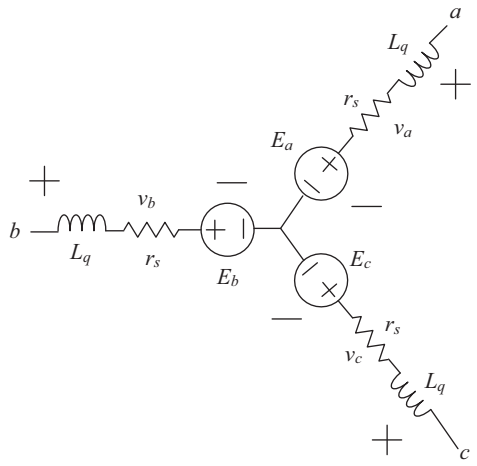

Fig. 1. Equivalent circuit corresponding to stator voltage equation (1).

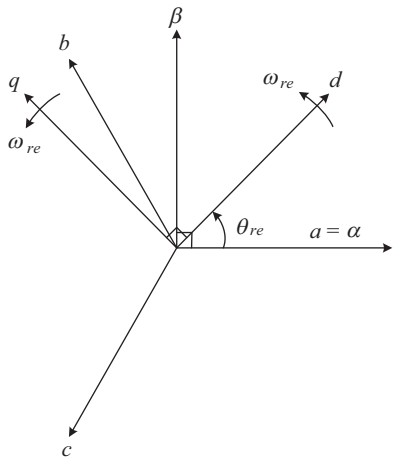

Fig. 2. Relationship between three coordinate systems.

with each detection interval equaling to half of the sampling period. In addition, a simple method to find the optimal switching mode is proposed to reduce the computational burden. Finally, for validation purpose, the method is realized through a microcontroller TMS320F28377S and applied to an interior permanent magnet synchronous motor (IPMSM) drive system with its feasibility and expected performance verified as well.

II. INTERIOR PERMANENT MAGNET SYNCHRONOUS MOTOR

The mathematical model of IPMSM is nonlinear and coupled. To reduce complexity, the stator voltage equation based on (Lin et al., 2014) can be expressed in the *a*-*b*-*c* coordinate frame as

$$v_x = r_s i_x + L_q \frac{di_x}{dt} + E_x,\ x \in \{a,b,c\} \tag{1}$$

where i_a, i_b, and i_c are stator currents; v_a, v_b, and v_c are stator voltages; E_a, E_b, and E_c are extended back EMFs (Lin et al., 2014); L_q is the *q*-axis equivalent inductance (Lin et al., 2014); r_s is the stator resistance and $\frac{d}{dt}$ stands for the differential operator. Fig. 1 shows the equivalent circuit corresponding to (1), and Fig. 2 depicts the relationships between three coordinate systems.

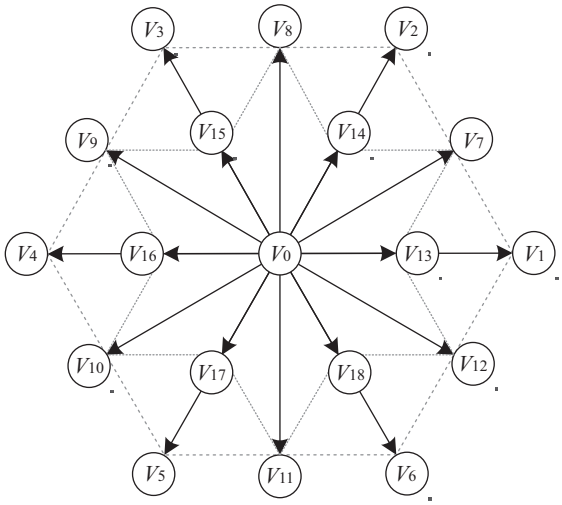

Fig. 3. 19 synthesized voltage vectors.

III. SIMPLIFIED TWO-SWITCHING-BASED MODEL PREDICTIVE CURRENT CONTROLLER (STSB-MPCC)

To help lower down computational burden, two voltage vectors (or two switching states) will be applied in a sampling period, each of the two voltage vectors (or two switching states) will be applied for half of the sampling period, i.e., $T_s/2$, respectively. Through the arrangements and combinations of two basic voltage vectors, 19 candidate switching modes, namely S_0~S_{18}, are generated and listed in Table 1, where the subscript "0" means that the upper-arm power switch is off and the lower-arm power switch is on, whereas the "1" used in switching function means that the upper-arm power switch is on and the lower-arm power switch is off. Fig. 3 illustrates these 19 synthesized voltage vectors. In contrast to the MPCC (Rodríguez et al., 2007) that uses 7 voltage vectors, the use of 19 synthesized voltage provides more flexibility as well as better prediction accuracy. To mitigate burden, the STSB-MPCC builds a searching rule to find the voltage vector yielding a minimum cost, which is fairly simple and helps to reduce the computational time. The searching rule involves four steps:

Step 1: Perform a wide range of search, and calculate the cost values associated with the six synthesized voltage vectors V_1~V_6.

Step 2: Choose a voltage vector from V_1~V_6.

Table 1. Correspondence between switching modes and synthesized voltage vectors.

Switching mode	Two switching states represented by two switching functions		Synthesized voltage vector
	First $T_s/2$	Second $T_s/2$	
S_0	(000)	(000)	$V_0 = V_0/2 + V_0/2$
S_1	(100)	(100)	$V_1 = V_1/2 + V_1/2$
S_2	(110)	(110)	$V_2 = V_2/2 + V_2/2$
S_3	(010)	(010)	$V_3 = V_3/2 + V_3/2$
S_4	(011)	(011)	$V_4 = V_4/2 + V_4/2$
S_5	(001)	(001)	$V_5 = V_5/2 + V_5/2$
S_6	(101)	(101)	$V_6 = V_6/2 + V_6/2$
S_7	(100)	(110)	$V_7 = V_1/2 + V_2/2$
S_8	(110)	(010)	$V_8 = V_2/2 + V_3/2$
S_9	(010)	(011)	$V_9 = V_3/2 + V_4/2$
S_{10}	(011)	(001)	$V_{10} = V_4/2 + V_5/2$
S_{11}	(001)	(101)	$V_{11} = V_5/2 + V_6/2$
S_{12}	(101)	(100)	$V_{12} = V_6/2 + V_1/2$
S_{13}	(100)	(000)	$V_{13} = V_1/2 + V_0/2$
S_{14}	(110)	(000)	$V_{14} = V_2/2 + V_0/2$
S_{15}	(010)	(000)	$V_{15} = V_3/2 + V_0/2$
S_{16}	(011)	(000)	$V_{16} = V_4/2 + V_0/2$
S_{17}	(001)	(000)	$V_{17} = V_5/2 + V_0/2$
S_{18}	(101)	(000)	$V_{18} = V_6/2 + V_0/2$

Table 2. STSB-MFPCC search table for the best voltage vector.

First selection V_{m1}, S_{m1}	Five alternative synthesized voltage vectors, switching modes				
	R_1	R_2	R_3	R_4	R_5
V_1, S_1	V_1, S_1	V_7, S_7	V_{12}, S_{12}	V_{13}, S_{13}	V_0, S_0
V_2, S_2	V_2, S_2	V_7, S_7	V_8, S_8	V_{14}, S_{14}	V_0, S_0
V_3, S_3	V_3, S_3	V_8, S_8	V_9, S_9	V_{15}, S_{15}	V_0, S_0
V_4, S_4	V_4, S_4	V_9, S_9	V_{10}, S_{10}	V_{16}, S_{16}	V_0, S_0
V_5, S_5	V_5, S_5	V_{10}, S_{10}	V_{11}, S_{11}	V_{17}, S_{17}	V_0, S_0
V_6, S_6	V_6, S_6	V_{11}, S_{11}	V_{12}, S_{12}	V_{18}, S_{18}	V_0, S_0

Step 3: Refine the search based on the result from Step 2. As an example, suppose V_2 from Step 2 is obtained, five synthesized voltage vectors V_2, V_7, V_8, V_{14}, and V_0 can then be found from Table 2.

Step 4: Select the switching mode that yields minimum cost. As an example, suppose V_{14} has the minimum cost among V_2, V_7, V_8, V_{14}, and V_0, the corresponding switching mode S_{14} is obtained by looking up Table 1.

Based on the algorithm of MPCC (Rodríguez et al., 2007), those 7 voltage vectors used therein can be replace by the 19 synthesized ones for STSB-MPCC. Step 1 and Step 2 can be expressed by the following:

$$g(k)_{V_{m1}\in\{V_1,\ldots,V_6\}} = \min\left\{g(k)_{V_1}, \ldots, g(k)_{V_6}\right\} \quad (2)$$

where g(k) is the kth cost function (defined in (Rodríguez et al., 2007)) evaluated at V_1~V_6, and V_{m1} appearing in (2) and Table 2 is the first synthesized voltage vector to be selected. Steps 3 and 4 described above can be represented by the following:

$$g(k)_{V_{m2}} = \min\left\{g(k)_{R_1}, g(k)_{R_2}, g(k)_{R_3}, g(k)_{R_4}, g(k)_{R_5}\right\} \quad (3)$$

where $V_{m_2} \in \{V_0, V_1, \ldots, V_{18}\}$ is the final synthesized voltage vector selected, $R_1 \in \{V_1, V_2, V_3, V_4, V_5, V_6\}$, $R_2 \in \{V_7, V_8, V_9, V_{10}, V_{11}\}$, $R_3 \in \{V_8, V_9, V_{10}, V_{11}, V_{12}\}$, $R_4 \in \{V_{13}, V_{14}, V_{15}, V_{16}, V_{17}, V_{18}\}$, and $R_5 \in \{V_0\}$. By looking up Table 1, the switching mode as obtained from (3) can be found. These two switching states will be sequentially applied in the next sampling period. The above four steps will significantly reduce the computational complexity and hence the burden of the digital signal controller.

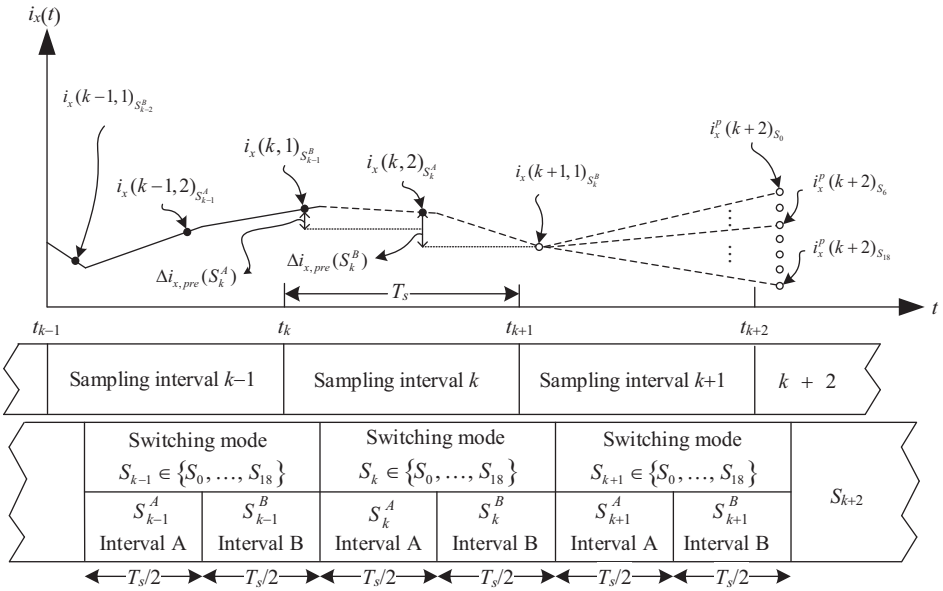

Fig. 4. Current difference predictions of STSB-MFPCC.

IV. SIMPLIFIED TWO-SWITCHING-BASED MODEL-FREE PREDICTIVE CURRENT CONTROLLER (STSB-MFPCC)

As mentioned above, through appropriate arrangement and combination of two switching states, 19 switching modes are generated as listed in Table 1. Conceptually, it is possible to improve the accuracy of current prediction further since each switching mode is composed of two switching states. In contrast to MFPCC (Lin et al., 2016) that detects current differences once in a sampling period, the proposed STSB-MFPCC measures current twice.

The current difference associated with the applied switching state can be calculated and recorded via a microcontroller or a digital signal processor (DSP) as shown in Fig. 4 where $i_x(k-1,1)$, $i_x(k-1,2)$, $i_x(k,1)$, $i_x(k,2)$, $i_x(k+1,1)$, and $i_x(k+1,2)$ are the first and second sampled currents in the $(k-1)$th, (k)th, and $(k+1)$th sampling periods, respectively where the subscript x stands for one of three phases. In the same figure, the individual switching state S^A_{k-1}, S^B_{k-1}, S^A_k, S^B_k, S^A_{k+1}, and S^B_{k+1} corresponds to one element of the set where the superscripts "A" and "B" stand for the switching intervals A and B, and the subscripts $k-1$, k, and $k+1$ represent the $(k-1)$th, kth, and $(k+1)$th sampling periods, respectively. The proposed searching rule in STSB-MPCC can be applied to STSB-MFPCC with only minor modification. The current differences associated with the switching states S^A_k, S^B_k, S^A_{k+1}, and S^B_{k+1} are defined as follows

$$\Delta i_x(S^A_k) = i_x(k,2) - i_x(k,1) \tag{4}$$

$$\Delta i_x(S^B_k) = i_x(k+1,1) - i_x(k,2) \tag{5}$$

$$\Delta i_x(S^A_{k+1}) = i_x(k+1,2) - i_x(k+1,1) \tag{6}$$

$$\Delta i_x(S^B_{k+1}) = i_x(k+2,1) - i_x(k+1,2) \tag{7}$$

See Fig. 4. Using (4)-(7), the future current to be sampled in the $(k+2)$th sampling period can be expressed as

$$\begin{aligned} i_x(k+2,1) = i_x(k,1) + \Delta i_x(S^A_k) + \Delta i_x(S^B_k) \\ + \Delta i_x(S^A_{k+1}) + \Delta i_x(S^B_{k+1}) \end{aligned} \tag{8}$$

It is assumed that the sampling period is short enough, or equivalently, the sampling frequency is high enough. It is also assumed that the current differences associated with different applied switching states during the sampling period are all linear. As such, the current differences defined in (4)-(7) can be approximated/replaced by their latest values with the same applied switching states, respectively. Namely, the following Eqs. (9)-(12) hold

$$\Delta i_x(S^A_k) \approx \Delta i_{x,pre}(S^A_k = S_e) \tag{9}$$

$$\Delta i_x(S^B_k) \approx \Delta i_{x,pre}(S^B_k = S_f) \tag{10}$$

$$\Delta i_x(S^A_{k+1}) \approx \Delta i_{x,pre}(S^A_{k+1} = S_g) \tag{11}$$

$$\Delta i_x(S^B_{k+1}) \approx \Delta i_{x,pre}(S^B_{k+1} = S_h) \tag{12}$$

with $S_e, S_f, S_g, S_h \in \{(000), (001), \ldots, (111)\}$, and the subscript "*pre*" means previous current difference. To reduce prediction error of (9)-(12), previous current difference will be replaced by the newly calculated one as shown below

$$\Delta i_{x,pre}(S_{k-1}^B) = i_x(k,1) - i_x(k-1,2) \tag{13}$$

The update frequency of (13) depends on the sampling period T_s, which means that shorter T_s will leads to higher update frequency. Given (9)-(12), the predicted value of (8) associated with the sampling mode S_{k+1} can be calculated by

$$\begin{aligned} i_x^p(k+2)_{S_{k+1}} = {} & i_x(k,1) + \Delta i_{x,pre}(S_k^A) + \Delta i_{x,pre}(S_k^B) \\ & + \Delta i_{x,pre}(S_{k+1}^A) + \Delta i_{x,pre}(S_{k+1}^B) \end{aligned} \tag{14}$$

where the superscript "*p*" stands for prediction. Next, a cost function is defined as

$$\begin{aligned} g(k)_{S_j} = {} & \left| i_a^*(k) - i_a^p(k+2)_{S_j} \right| + \left| i_b^*(k) - i_b^p(k+2)_{S_j} \right| \\ & + \left| i_c^*(k) - i_c^p(k+2)_{S_j} \right| \end{aligned} \tag{15}$$

where $S_j \in \{S_0, S_1, \ldots, S_{18}\}$. Based on (15), 19 cost values can be computed as there are 19 candidate switching modes. It will, however, increase the computational burden of the DSP/microcontroller. To circumvent this problem, only 11 cost values will be considered. First, six candidates are calculated to find the lowest one, i.e.,

$$g(k)_{S_{m1}} = \min \left\{ \begin{matrix} g(k)_{S_1}, g(k)_{S_2}, g(k)_{S_3}, \\ g(k)_{S_4}, g(k)_{S_5}, g(k)_{S_6} \end{matrix} \right\}. \tag{16}$$

Next, five switching modes will be considered in the second search according to Table 2. The corresponding switching mode with the lowest cost value then can be found by

$$g(k)_{S_{m2}} = \min \left\{ \begin{matrix} g(k)_{N_1}, g(k)_{N_2}, g(k)_{N_3}, \\ g(k)_{N_4}, g(k)_{N_5} \end{matrix} \right\} \tag{17}$$

where $S_{m_2} \in \{S_0, S_1, \ldots, S_{18}\}$, $N_1 \in \{V_1, V_2, V_3, V_4, V_5, V_6\}$, $N_2 \in \{V_7, V_8, V_9, V_{10}, V_{11}\}$, $N_3 \in \{V_8, V_9, V_{10}, V_{11}, V_{12}\}$, $N_4 \in \{V_{13}, V_{14}, V_{15}, V_{16}, V_{17}, V_{18}\}$, and $N_5 \in \{V_0\}$.

Finally, the selected switching mode consisting of two switching states as listed in Table 1 will be transmitted to control the six power switches of the inverter (ON/OFF) in the next sampling period.

V. EXPERIMENTS

Table 3. Specifications of the IPMSM.

Parameter	Value	Unit
Poles	4	Pole
Rated power	375	W
Rated speed	3000	rpm
Stator resistance	6.8	Ω
d-axis inductance	24.76	mH
q-axis inductance	45.33	mH

Table 4. Specifications of the inverter SCM1246MF.

Parameter	Rating value	Unit
Output current	30	A
Output current (pulse)	45	A
Logic supply voltage	20	V
Isolation voltage (for 1 min)	2500	V
Main supply voltage (DC)	450	V
Main supply voltage (surge)	500	V
IGBT breakdown voltage	600	V

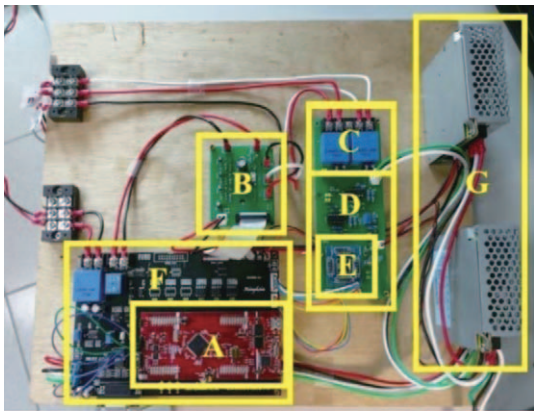

(a)

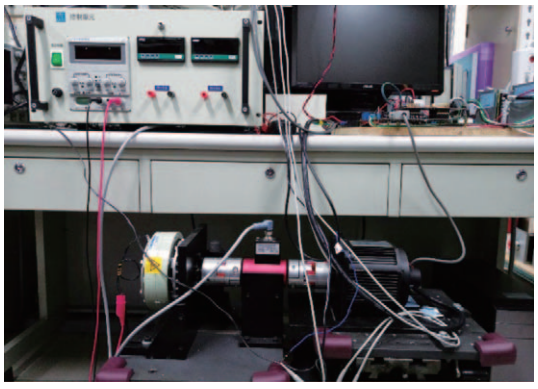

(b)

Fig. 5. (a) Voltage source inverter system; (b) IPMSM drive system.

An experimental setup for an IPMSM is developed wherein a DSP TMS320F28377S is utilized with its sampling period T_s

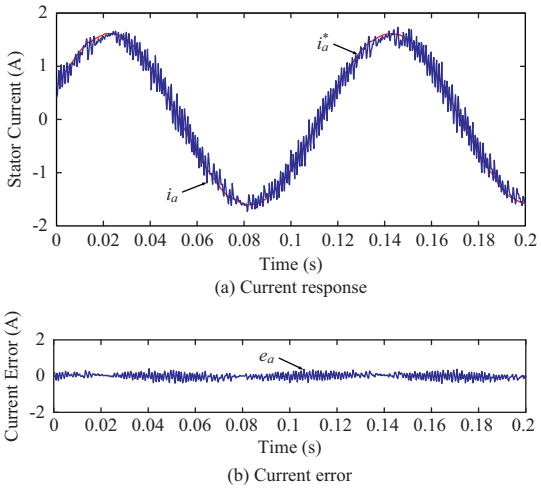

Fig. 6. Experimental results of the MPCC under 0.8 Nm load and 500 rpm.

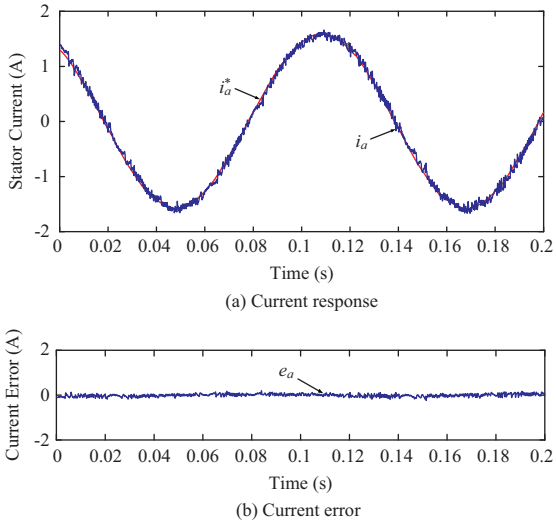

Fig. 8. Experimental results of the MFCC under 0.8 Nm load and 500 rpm.

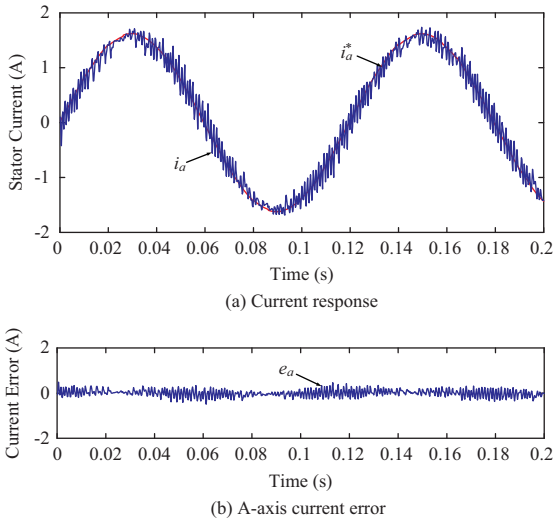

Fig. 7. Experimental results of the STSB-MPCC under 0.8 Nm load and 500 rpm.

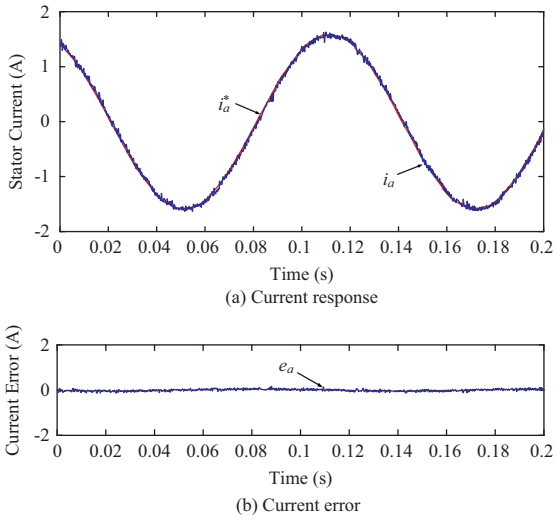

Fig. 9. Experimental results of the STSB-MFPCC under 0.8 Nm load and 500 rpm.

set as 100 μs. The parameters, as listed in Table 3, are $L_d = 24.76$ mH, $L_q = 45.33$ mH, and $r_s = 6.8\ \Omega$. The drive system, shown in Fig. 5, comprises 9 blocks including (a) TMS320F28337S digital signal controller, (b) SCM1246MF intelligent power module, (c) current sensing circuit, (d) current/voltage conversion circuit, (e) 16-bit analog/digital converter, (f) overcurrent protection circuit and optical isolation circuit, (g) power supplier, (h) interior permanent magnet synchronous motor, and (i) load test equipment. Given in Table 4 are the parameters of SCM1246MF.

Two performance measures are adopted in this paper to quantify the experimental results; they are the average current error, (denoted e_{ace}) and the average current ripple (denoted e_{acr}). The former is defined as

$$e_{ace} = \frac{1}{N}\left(\sum_{k=1}^{N}\left|i_a^*[k] - i_a[k]\right|\right) \tag{18}$$

where the superscript * represents current command, and N is the number of samples. The latter is defined as

$$e_{acr} = \left(\sqrt{\frac{1}{N}\sum_{k=1}^{N}\left(i_a^*[k] - i_a[k]\right)^2}\right) \tag{19}$$

Figs. 6-13 show the current-tracking performances of the MPCC (Rodríguez et al., 2007), STSB-MPCC, MFPCC (Lin et al., 2014), and STSB-MFPCC with the IPMSM operated at 500 rpm and 1000rpm under a load of 0.8 Nm, respectively, where e_a represents a-phase current error. The experimental results in Figs. 6-13 is to show the current responses of different PCCs under close-loop speed control which is proportional-

Table 5. Numeric values of two performance measures based on experimental results of Figs. 6-9.

PCC scheme	e_{ace} (A)	e_{acr} (A)
MPCC	0.1166	0.1464
STSB-MPCC	0.1167	0.148
MFPCC	0.0549	0.0681
STSB-MFPCC	0.0378	0.047

Table 6. Numeric values of two performance measures based on experimental results of Figs. 10-13.

PCC scheme	e_{ace} (A)	e_{acr} (A)
MPCC	0.2691	0.3376
STSB-MPCC	0.257	0.3247
MFPCC	0.1334	0.1646
STSB-MFPCC	0.1	0.1204

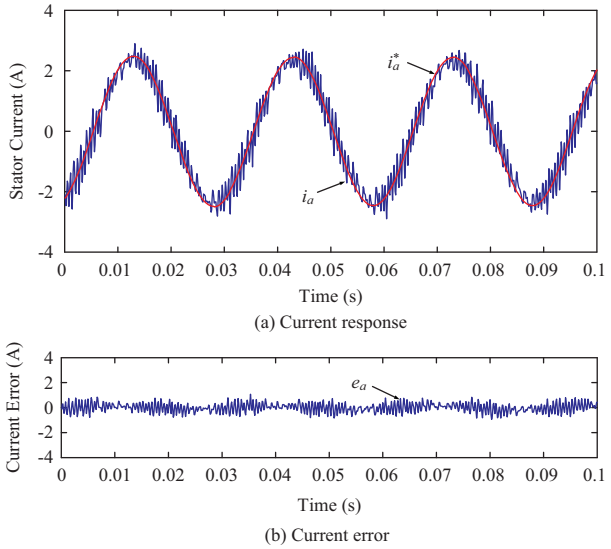

Fig. 10. Experimental results of the MPCC under 0.8 Nm load and 1000 rpm.

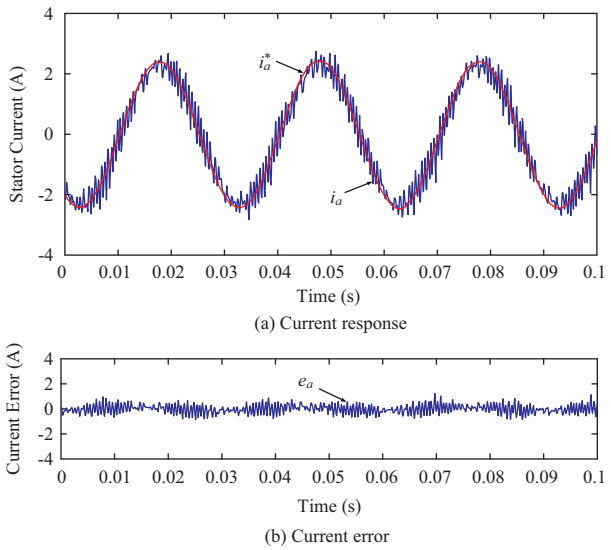

Fig. 11. Experimental results of the STSB-MPCC under 0.8 Nm load and 1000 rpm.

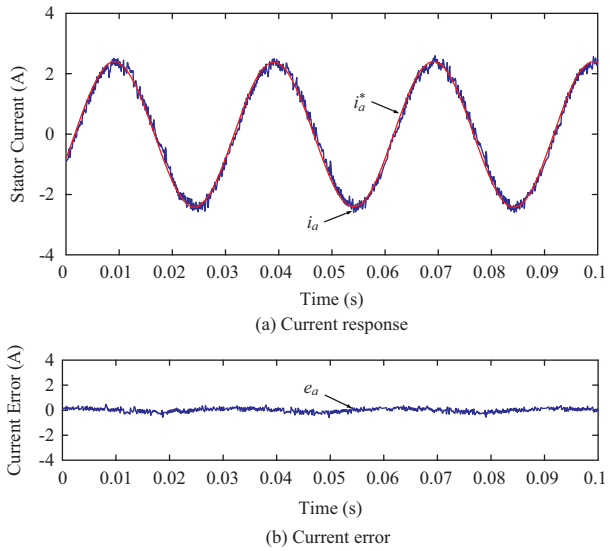

Fig. 12. Experimental results of the MFCC under 0.8 Nm load and 1000 rpm.

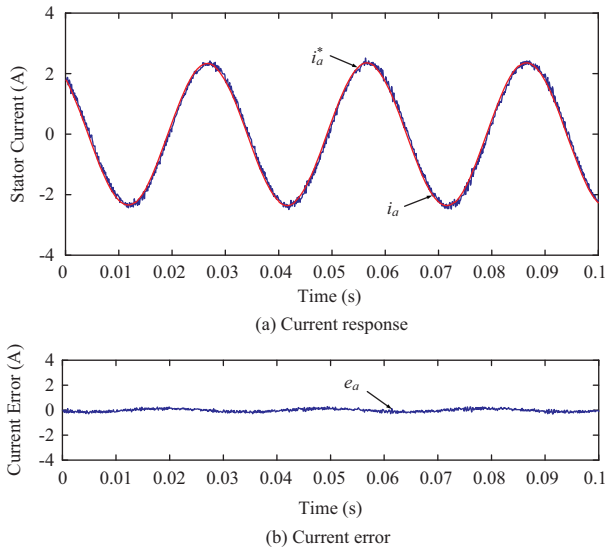

Fig. 13. Experimental results of the STSB-MFPCC under 0.8 Nm load and 1000 rpm.

integral (PI) based with speed error as its input and q-axis current command as the output. After a coordinate transformation (d-q to a-b-c), the a-axis, b-axis and c-axis current commands can be obtained. The parameters of PI controller in the speed loop, as of Figs. 6-13, remain unchanged for fair comparison purpose. It can be seen from these figures that different PCCs exhibit different current-tracking outcomes. Numeric values of the two performance measures, as defined by (18) and (19), are listed in

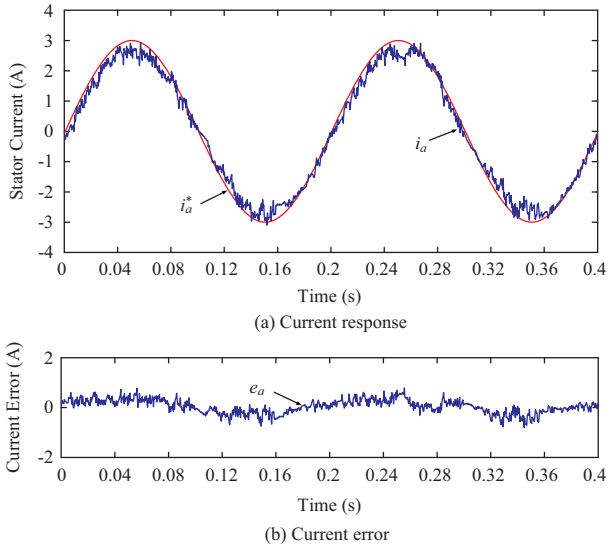

Fig. 14. Experimental results of the MPCC tracking current command 3 A and frequency 5 Hz.

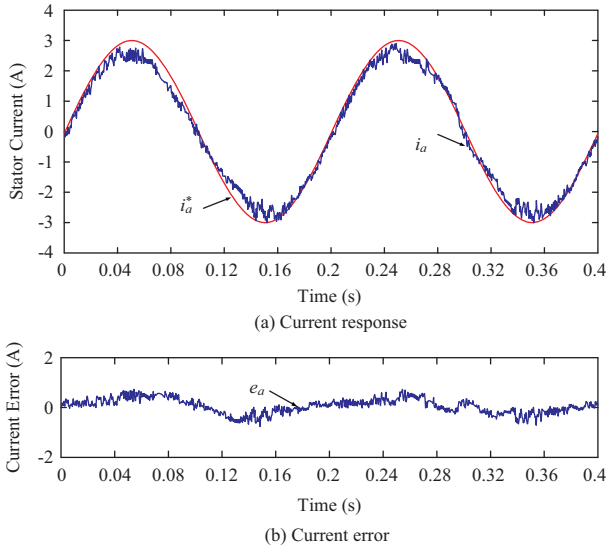

Fig. 15. Experimental results of the STSB-MPCC tracking current command 3 A and frequency 5 Hz.

Table 5 for comparison purpose. One can see from Figs. 6-13 and Tables 5 and 6 that the STSB-MFPCC has minimum average current error and minimum average current ripple as opposed to MPCC (Rodríguez et al., 2007), STSB-MPCC, and MFPCC (Lin et al., 2014). Next, a current command with an amplitude of 3 A and a frequency of 5 Hz is used, replacing the output of speed controller, to test the current response of the four PCCs whose results are shown in Figs. 14-17. From the measured waveforms, it can be confirmed that the proposed STSB-MFPCC and STSB-MPCC enhance the performances of the MFPCC (Lin et al., 2014) and MPCC (Rodríguez et al., 2007). Similar conclusion can also be drawn from Table 7 that the proposed method outperforms the other PCCs. Next, the experimental results shown

Table 7. Numeric values of two performance measures based on experimental results of Figs. 14-17.

PCC scheme	e_{ace} (A)	e_{acr} (A)
MPCC	0.231	0.2873
STSB-MPCC	0.251	0.3086
MFPCC	0.167	0.2835
STSB-MFPCC	0.08	0.1

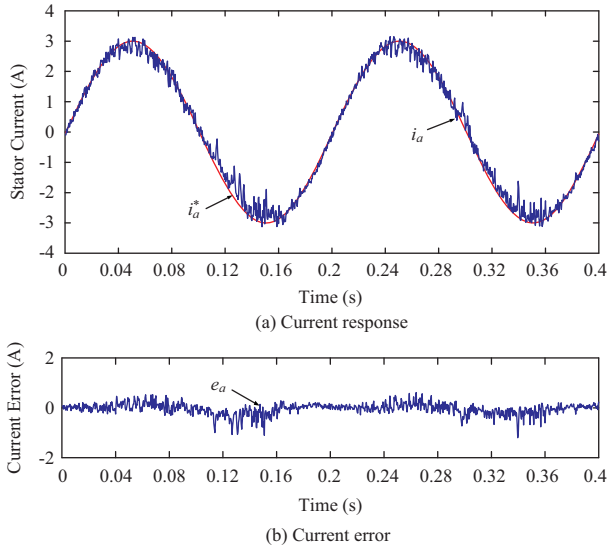

Fig. 16. Experimental results of the MFPCC tracking current command 3 A and frequency 5 Hz.

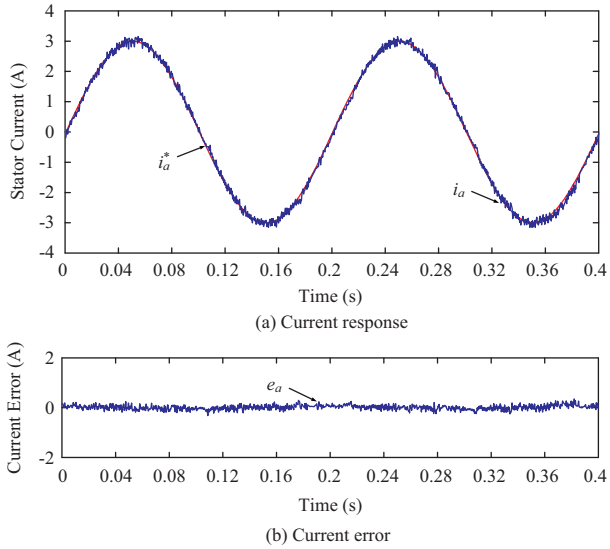

Fig. 17. Experimental results of the STSB-MFPCC tracking current command 3 A and frequency 5 Hz.

in Figs. 18-21 are to demonstrate the transient responses of the four PCCs, i.e., by tracking sinusoidal current commands with a frequency of 10 Hz and amplitudes jumping from 1 A to 4 A at 0.1 sec. As one can observe, the current errors and ripples of

Table 8. Numeric values of two performance measures based on experimental results of Figs. 18-21.

PCC scheme	e_{ace} (A)	e_{acr} (A)
MPCC	0.2125	0.3513
STSB-MPCC	0.204	0.3306
MFPCC	0.0994	0.2047
STSB-MFPCC	0.0752	0.1746

Table 9. Computation time of the TMS320F28377S microcontroller for different PCC schemes.

PCC scheme	Computation time (μs)
MPCC	20.2
STSB-MPCC	25.3
MFPCC	19.7
STSB -MFPCC	33.5

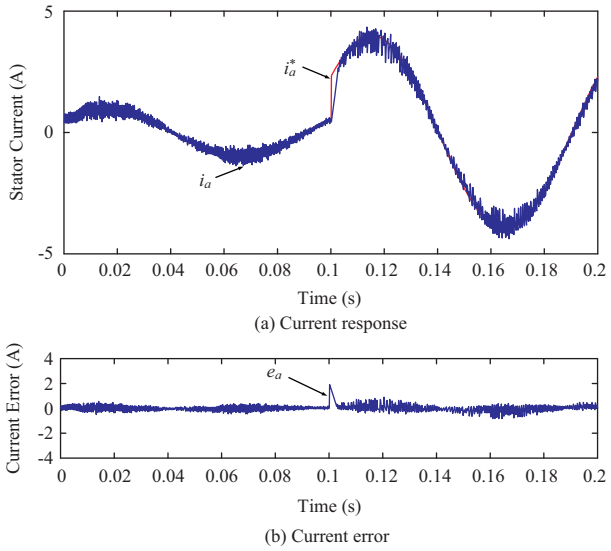

Fig. 18. Experimental results of the MPCC tracking a 10 Hz sinusoidal current command with amplitude jumping from 1 A to 4 A at 0.1 sec.

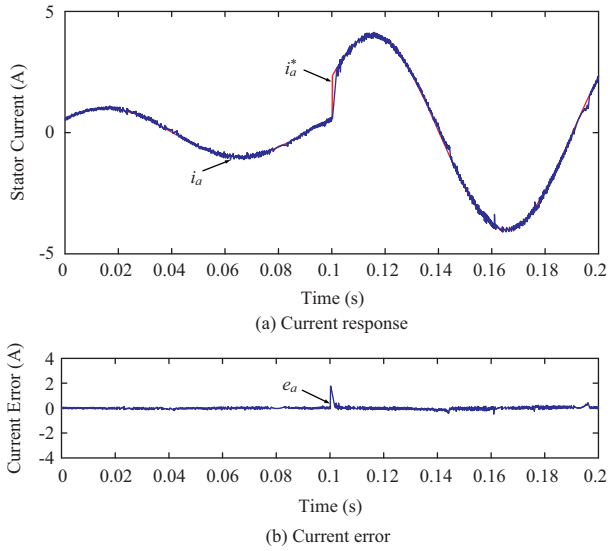

Fig. 20. Experimental results of the MFPCC tracking a 10 Hz sinusoidal current command with amplitude jumping from 1 A to 4 A at 0.1 sec.

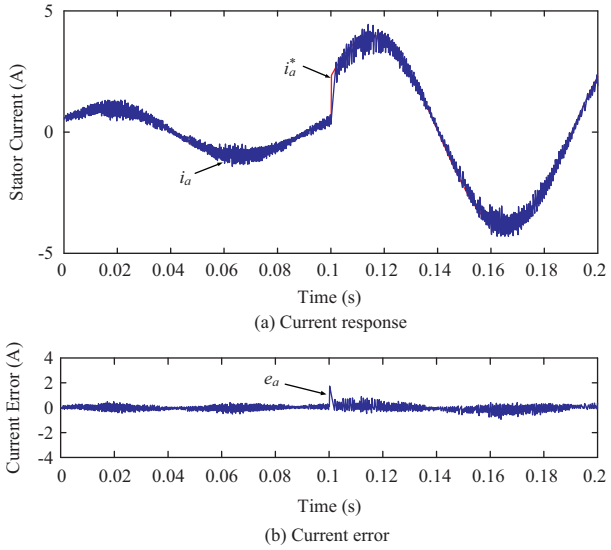

Fig. 19. Experimental results of the STSB-MPCC tracking a 10 Hz sinusoidal current command with amplitude jumping from 1 A to 4 A at 0.1 sec.

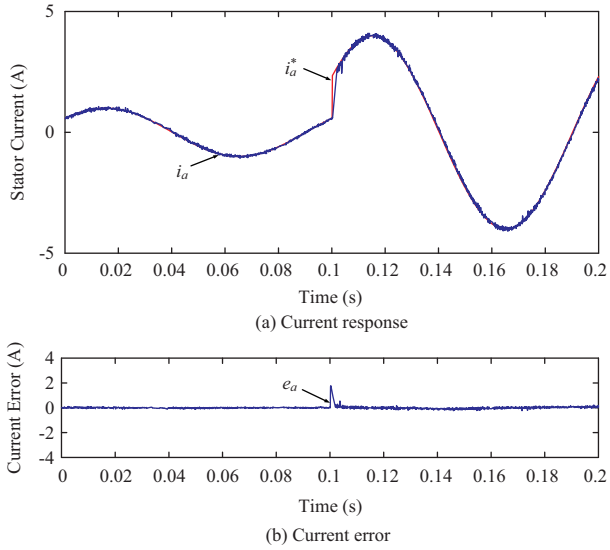

Fig. 21. Experimental results of the STSB-MFPCC tracking a 10 Hz sinusoidal current command and amplitude jumping from 1 A to 4 A at 0.1 sec.

the MFPCC (Lin et al., 2014) and the STSB-MFPCC right after the *a*-axis current command changing at 0.1 second are significantly smaller than that of the MPCC (Rodríguez et al., 2007) and the STSB-MPCC. As of the two performance measures, one may see from Table 8 that the proposed control has the smallest values. Table 9 summarizes the computation time of

the four PCCs, demonstrating that they can be executed within 100 microseconds. Although the proposed method requires more computation time, this small drawback can be compensated by the high-performance microcontroller TMS320F28377S used. In addition, using a high-performance A\D converter with a high bandwidth for data conversion, one can effectively reduce the time required to read in the current values. In summary, the experimental results shown in Figs. 6-21 and Tables 5-8 demonstrate that the proposed approach has better steady-state and transient responses in current-tracking compared to that of the MPCC (Rodríguez et al., 2007), STSB-MPCC, and MFPCC (Lin et al., 2014).

VI. CONCLUSION

For predictive current control, the proposed STSB-MFPCC in this work does not require the information about resistance, inductance, and back electromotive force, nor the system model. Two basic switching states (voltage vectors) are applied, and current variations are updated twice within a sampling period leading to significant accuracy enhancement. Besides, the computation burden of the STSB-MFPCC, in comparison with that of the TSB-MPCC, is effectively reduced thanks to a simplified search scheme. In terms of performance, the proposed approach is better than the MPCC, MFPCC, and STSB-MPCC as verified by the provided experimental results.

ACKNOWLEDGEMENTS

This manuscript is a result of joint research sponsored by the Ministry of Science and Technology of Taiwan, National Taiwan Ocean University, Chung Yuan Christian University, and National Taipei University of Technology under grant numbers MOST 107-2221-E-019-040, MOST 107-2221-E-033-062, and USTP-NTUT-NTOU-107-01. The authors thank these institutions for their support.

REFERENCES

Bolognani, S., R. Kennel, S. Kuehl and G. Paccagnella (2011). Speed and current model predictive control of an IPM synchronous motor drive. Proceeding of the 2011 IEEE International Electric Machines & Drives Conference, Niagara Falls, ON, Canada, 1579-1602.

Chen, Y., T.-H. Liu, C.-F. Hsiao and C.-K. Lin (2015). Implementation of adaptive inverse controller for an interior permanent magnet synchronous motor adjustable speed drive system based on predictive current control. IET Electric Power Applications 9, 60-70.

Gu, M., S. Ogasawara and M. Takemoto (2016). Novel PWM schemes with multi SVPWM of sensorless IPMSM drives for reducing current ripple. IEEE Transactions on Power Electronics 31, 6461-6475.

Kadota, M., S. Lerdudomsak, S. Doki and S. Okuma (2007). A novel current control system of IPMSM operating at high speed based on model predictive control. Proceeding of the 2007 Power Conversion Conference, Nagoya, Japan, 1315-1319.

Lin, C. K., J.-t. Yu, Y.-S. Lai, H.-C. Yu, Y.-H. Lin and F.-M. Chen (2016). Simplified model-free predictive current control for interior permanent magnet synchronous motors. Electronics Letters 52, 49-50.

Lin, C.-K., J.-T. Yu, H.-Q. Huang, J.-T. Wang, H.-C. Yu and Y.-S. Lai (2018). A dual-voltage-vector model-free predictive current controller for synchronous reluctance motor drive systems. Energies 11, 1743.

Lin, C.-K., T.-H. Liu, J.-t. Yu, L.-C. Fu and C.-F. Hsiao (2014). Model-free predictive current control for interior permanent magnet synchronous motor drives based on current difference detection technique. IEEE Transactions on Industrial Electronics 61, 667-681.

Lin, C.-K., T.-H. Yu, Y.-S. Lai, H.-C. Yu and C.-I. Peng (2016). Two-vector-based modeless predictive current control for four-switch inverter-fed synchronous reluctance motors emulating the six-switch inverter operation. Electronics Letters 52, 1244-1246.

Lin, J., C. Gong, Z. Han and H. Yu (2018). IPMSM model predictive control in flux-weakening operation using an improved algorithm. IEEE Transactions on Industrial Electronics 65, 9378-9387.

Mwasilu, F., E.-K. Kim, M. S. Rafaq and J.-W. Jung (2018). Finite-set model predictive control scheme with an optimal switching voltage vector technique for high-performance IPMSM drive applications. IEEE Transactions on Industrial Informatics 14, 3840-3848.

Rodríguez, J., J. Pontt, C. Silva, A. S. Csar, P. Correa, P. Lezana, P. Cortes and U. Ammann (2007). Predictive current control of a voltage source inverter. IEEE Transactions on Industrial Electronics 54, 495-503.

Zhang, Y., L, Huang, D. Xu, J. Liu and J. Jin (2018). Performance evaluation of two-vector-based model predictive current control of PMSM drives. Chinese Journal of Electrical Engineering 31, 65-81.